Inorg. Chem. **2007**, *46*, 8963–8970

Correlation of Metal Spin-State in α-Diimine Iron Catalysts with Polymerization Mechanism

Laura E. N. Allan, Michael P. Shaver, Andrew J. P. White, and Vernon C. Gibson*

Contribution from the Department of Chemistry, Imperial College London, South Kensington, London, SW7 2AZ, UK

Received July 27, 2007

The α-diimine iron complexes, $^{R',R''}$[*N,N*]$FeCl_2$ ($^{R',R''}$[*N,N*] = R′–N═CR″–CR″═N–R′, where R′ = *tert*-butyl (*t*Bu), cyclohexyl (Cy) and R″ = phenyl (Ph), *para*-fluorophenyl (F–Ph), *para*-bromophenyl (Br–Ph), *para*-methylphenyl (Me–Ph), or *para*-methoxyphenyl (MeO–Ph)), are found to polymerize styrene through a catalytic chain transfer (CCT) mechanism. Magnetic moment measurements indicate that Fe(III) complexes containing these ligands possess intermediate ($S = {}^3/_2$) spin-state iron centers. In contrast, Fe(III) complexes bearing proton (R″ = H) and *para*-dimethylaminophenyl (R″ = NMe_2–Ph) substituents are high-spin and are efficient atom transfer radical polymerization (ATRP) catalysts. Hammett plots show a linear correlation of the substituent constant, σ, with polymerization rate and polymer molecular weight, respectively.

Introduction

Despite the widely recognized and important influence of metal spin-state on the metal-centered reactivity of enzymes,[1−5] the effect of metal spin-state on metal-based reactivity in nonbiological systems remains largely undocumented. Recently, we identified and reported a correlation between metal spin-state and the nature of the resultant polymer in a metal-catalyzed radical polymerization system. We concluded that differing mechanistic pathways had been followed, depending upon the spin-state adopted by the catalyst system, the latter being determined by the ligand substituents.[6]

Polymerizations mediated by α-diimine Fe(II) complexes bearing alkylimine substituents, in which the parent Fe(III) complex is in a high spin ($S = {}^5/_2$) state, afforded controlled polymerizations of styrene via an atom transfer radical polymerization (ATRP) mechanism, whereas arylimine-based systems, with the corresponding Fe(III) species in an intermediate ($S = {}^3/_2$) spin-state, followed a catalytic chain transfer (CCT) mechanism.[7−9] The isolated polymer provides a record of the individual catalytic events, with molecular weights and polymer end-groups providing a signature of the prevalent mechanism.

ATRP is a facile, pseudo-living radical polymerization, which uses metal-mediated halogen exchange to control the equilibrium between active and dormant polymer chains.[10,11] By ensuring that the majority of species lie on the dormant side of this dynamic equilibrium, the radical concentration remains low. This minimizes bimolecular termination reactions and generates halogen-terminated polymer chains with molecular weights very close to theoretical values, increasing linearly with conversion and displaying low polydispersities. Whereas copper[12] and ruthenium[13] are the most extensively studied metals in ATRP catalysis, a wide range of other metals have also been shown to be active, including nickel,[14−20] palladium,[21,22] rhodium,[23,24] molybdenum,[25−32]

* To whom correspondence should be addressed. E-mail: v.gibson@imperial.ac.uk.

(1) Williams, R. J. P. *Fed. Proc. Fed. Am. Soc. Exp. Biol.* **1961**, *20*, 5.
(2) Hoard, J. L.; Hoard, M. J.; Hamor, T. A.; Caughey, W. S. *J. Am. Chem. Soc.* **1965**, *87*, 2312.
(3) Scheidt, W. R.; Reed, C. A. *Chem. Rev.* **1981**, *81*, 543.
(4) Perutz, M. F.; Wilkinson, A. J.; Paoli, M.; Dodson, G. G. *Ann. Rev. Biophys. Biomol. Struct.* **1998**, *27*, 1 and references therein.
(5) Meunier, B.; deVisser, S. P.; Shaik, S. *Chem. Rev.* **2004**, *104*, 3947.
(6) Shaver, M. P.; Allan, L. E. N.; Rzepa, H. S.; Gibson, V. C. *Angew. Chem., Int. Ed.* **2006**, *45*, 1241.
(7) Gibson, V. C.; O'Reilly, R. K.; Reed, W.; Wass, D.; White, A. J. P.; Williams, D. J. *Chem. Commun.* **2002**, 1850.
(8) Gibson, V. C.; O'Reilly, R. K.; Wass, D. F.; White, A. J. P.; Williams, D. J. *Macromolecules* **2003**, *36*, 2591.
(9) O'Reilly, R. K. Synthesis of Novel Iron Complexes and their use in Atom Transfer Radical Polymerisation. Ph.D. Thesis, University of London, 2003.
(10) Matyjaszewski, K.; Xia, J. *Chem. Rev.* **2001**, 101, 2921.
(11) Kamigaito, M.; Ando, T.; Sawamoto, M. *Chem. Rev.* **2001**, *101*, 3689.
(12) Pintauer, T.; Matyjaszewski, K. *Coord. Chem. Rev.* **2005**, *249*, 1155.
(13) Kamigaito, M.; Ando, T.; Sawamoto, M. *The Chemical Record* **2004**, *4*, 159.
(14) Granel, C.; Dubois, P.; Jérome, R.; Teyssié, P. *Macromolecules* **1996**, 29, 8576.
(15) Li, P.; Qiu, K.-Y. *Polymer* **2002**, *43*, 5873.

10.1021/ic701500y CCC: $37.00
Published on Web 09/14/2007

iron,[7,33−39] and rhenium.[40,41] More recently, systems based on titanium,[42,43] cobalt,[44] and osmium[45] have been added.

CCT is an efficient method for synthesizing low-molecular-weight polymers via a free-radical mechanism.[46,47] It is generally thought that the mechanism proceeds via a two-step process, involving hydrogen abstraction by the metal center and then subsequent reinitiation through monomer insertion into the metal−hydrogen bond.[48−50] It is also possible for the metal hydride species to be formed via trapping of the alkyl radical to give initially an organometallic intermediate, which then undergoes a β-H elimination process to release the olefin.[51,52] The first part of this latter process forms the basis of the organometallic-mediated radical polymerization (OMRP) reaction, which, when combined with the β-H elimination step, results overall in the CCT pathway (Scheme 1). A separate study in our laboratory has focused on the organometallic intermediates in the α-diimine iron system and their use in OMRP.[53]

Scheme 1

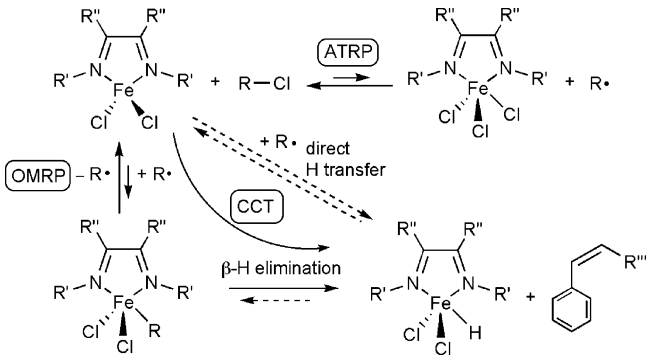

ATRP and CCT polymerization mechanisms are not mutually exclusive; they are intimately linked by the equilibria illustrated in Scheme 1. Various factors can play a role in determining whether a polymerization catalyzed by a particular complex will occur via the predominantly halogenophilic ATRP route, whether the OMRP equilibrium will dominate, or whether hydrogen transfer will occur to give CCT products. Such competing mechanisms have been observed by Poli and co-workers with the half-sandwich molybdenum compounds, $CpMoCl_2(PMe_3)_2$ and $CpMoCl_2$-(dppe), which are active catalysts for the polymerization of styrene under both ATRP and OMRP conditions.[25,26] $CpMoCl_2(C_4H_6)$ and $CpMo(SiMe_3)_2(C_4H_6)$, however, afford short-chain, olefin-terminated oligomers via an overall CCT process. A recent minireview discusses the interplay between these one-electron processes.[54]

The correlation of the metal spin-state with the mechanistic outcome in catalytic polymerization using α-diimine Fe(II) complexes remains the first reported example of its kind. Initially, we found that the spin-state is strongly influenced by the imine *N*-donor substituents, with alkylimine donors affording high-spin Fe(III) species, whereas arylimine derivatives gave intermediate-spin Fe(III) species.[7,8] Subsequently, we found that aryl substituents attached to the carbon atoms of the imine backbone can also affect the spin-state of the iron centers, as a result of extensive delocalization throughout the ligand backbone.[6] Here, we present the results of our studies on Fe(II) and Fe(III) complexes that bear α-diimine ligands with differing para-substituted aryl groups attached to the backbone carbon atoms, along with a study of their behavior in catalytic polymerization.

(16) Moineau, G.; Minet, M.; Dubois, P.; Teyssié, P.; Senninger, T.; Jérôme, R. *Macromolecules* **1999**, *32*, 27.
(17) Uegaki, H.; Kotani, Y.; Kamigaito, M.; Sawamoto, M. *Macromolecules* **1997**, *30*, 2249.
(18) Uegaki, H.; Kotani, Y.; Kamigaito, M.; Sawamoto, M. *Macromolecules* **1998**, *31*, 6756.
(19) Uegaki, H.; Kamigaito, M.; Sawamoto, M. *J. Polym. Sci., Part A: Polym. Chem.* **1999**, *37*, 3003.
(20) O'Reilly, R. K.; Shaver, M. P.; Gibson, V. C. *Inorg. Chim. Acta* **2006**, *359*, 4417.
(21) Lecomte, P.; Drapier, I.; Dubois, P.; Tessiyé, P.; Jérome, R. *Macromolecules* **1997**, *30*, 7631.
(22) Hong, S. C.; Jia, S.; Teodorescu, M.; Kowalewski, T.; Matyjaszewski, K.; Gottfried, A.; Brookhart, M. *J. Polym. Sci., Part A: Polym. Chem.* **2002**, *40*, 2736.
(23) Percec, V.; Barboiu, B.; Neumann, A.; Ronda, J. C.; Zhao, M. *Macromolecules* **1996**, *29*, 3665.
(24) Moineau, G.; Granel, C.; Dubois, P.; Teyssié, P.; Jérôme, R. *Macromolecules* **1998**, 31, 542.
(25) Grognec, E. L.; Claverie, J.; Poli, R. *J. Am. Chem. Soc.* **2001**, *123*, 9513.
(26) Stoffelbach, F.; Poli, R.; Richard, P. *J. Organomet. Chem.* **2002**, *663*, 269.
(27) Stoffelbach, F.; Claverie, J.; Poli, R. *C.R. Acad. Sci., Ser. IIc: Chim.* **2002**, *5*, 37.
(28) Stoffelbach, F.; Haddleton, D. M.; Poli, R. *Eur. Polym. J.* **2003**, *39*, 2099.
(29) Poli, R.; Stoffelbach, F.; Maria, S.; Mata, J. *Chem.—Eur. J.* **2005**, *11*, 2537.
(30) Maria, S.; Stoffelbach, F.; Mata, J.; Daran, J.-C.; Richard, P.; Poli, R. *J. Am. Chem. Soc.* **2005**, *127*, 2537.
(31) Mata, J.; Maria, S.; Daran, J.-C.; Poli, R. *Eur. J. Inorg. Chem.* **2006**, *13*, 2624.
(32) Stoffelbach, F.; Richard, P.; Poli, R.; Jenny, T.; Savary, C. *Inorg. Chim. Acta* **2006**, *359*, 4447.
(33) Ando, T.; Kamigaito, M.; Sawamoto, M. *Macromolecules* **1997**, *30*, 4507.
(34) Fuji, Y.; Ando, T.; Kamigaito, M.; Sawamoto, M. *Macromolecules* **2002**, *35*, 2949.
(35) Gibson, V. C.; O'Reilly, R. K.; White, A. J. P.; Williams, D. J. *J. Am. Chem. Soc.* **2003**, *125*, 8450.
(36) Ibrahim, K.; Lofgren, B.; Seppala, J. *Eur. Polym. J.* **2003**, *39*, 939.
(37) Louie, J.; Grubbs, R. H. *Chem. Commun.* **2000**, *16*, 1479.
(38) Kotani, Y.; Kamigaito, M.; Sawamoto, M. *Macromolecules* **1999**, *32*, 6877.
(39) Matyjaszewski, K.; Wei, M.; Xia, J.; McDermott, N. E. *Macromolecules* **1997**, *30*, 8161.
(40) Kotani, Y.; Kamigaito, M.; Sawamoto, M. *Macromolecules* **1999**, *32*, 2420.
(41) Kotani, Y.; Kamigaito, M.; Sawamoto, M. *Macromolecules* **2000**, *33*, 6746.
(42) Kabachii, Y. A.; Kochev, S. Y.; Bronsteinl, L. M.; Blagodatskikh, I. B.; Valetsky, P. M. *Polym. Bull.* **2003**, *50*, 271.
(43) Grishin, D. F.; Semyonycheva, L. L.; Telegina, E. V.; Smirnov, A. S.; Nevodchikovc, V. I. *Russ. Chem. Bull., Int. Ed.* **2003**, *52*, 505.
(44) Weiser, M. S.; Lhaupt, R. M. *J. Polym. Sci., Part A: Polym. Chem.* **2005**, *43*, 3804.
(45) Braunecker, W. A.; Itami, Y.; Matyjaszewski, K. *Macromolecules* **2005**, *38*, 9402.
(46) Gridnev, A. *J. Polym. Sci., Polym. Chem. Ed.* **2000**, *38*, 1753.
(47) Gridnev, A.; Ittel, D. S. *Chem. Rev.* **2001**, *101*, 3611.
(48) Enikolopyan, N. S.; Smirnov, B. R.; Ponomarev, G. V.; Bel'govskii, I. M. *J. Polym. Sci., Polym. Chem. Ed.* **1981**, *19*, 879.
(49) Burczyk, A. F.; O'Driscoll, K. F.; Rempel, G. L. *J. Polym. Sci., Polym. Chem. Ed.* **1984**, *22*, 3255.
(50) Gridnev, A. A.; Ittel, S. D.; Fryd, M.; Wayland, B. B. *Organometallics* **1993**, *12*, 4871.
(51) Gridnev, A. A.; Ittel, S. D.; Wayland, B. B.; Fryd, M. *Organometallics* **1996**, *15*, 5116.
(52) Heuts, J. P. A.; Forster, D. J.; Davis, T. P. *Macromolecules* **1999**, *32*, 2511.
(53) Shaver, M. P.; Allan, L. E. N.; Gibson, V. C. *Organometallics* **2007**, *26*, 4725.
(54) Poli, R. *Angew. Chem., Int. Ed.* **2006**, *45*, 5058.

Scheme 2

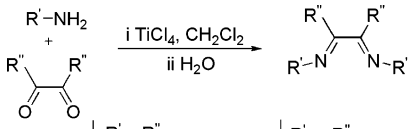

	R′	R″		R′	R″
1	Cy	Ph	**7**	^{t}Bu	Ph
2	Cy	F-Ph	**8**	^{t}Bu	F-Ph
3	Cy	Br-Ph	**9**	^{t}Bu	Br-Ph
4	Cy	Me-Ph	**10**	^{t}Bu	Me-Ph
5	Cy	MeO-Ph	**11**	^{t}Bu	MeO-Ph
6	Cy	NMe_2-Ph	**12**	^{t}Bu	NMe_2-Ph

Scheme 3

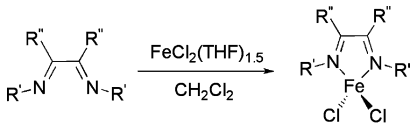

	R′	R″		R′	R″
13	Cy	Ph	**19**	^{t}Bu	Ph
14	Cy	F-Ph	**20**	^{t}Bu	F-Ph
15	Cy	Br-Ph	**21**	^{t}Bu	Br-Ph
16	Cy	Me-Ph	**22**	^{t}Bu	Me-Ph
17	Cy	MeO-Ph	**23**	^{t}Bu	MeO-Ph
18	Cy	NMe_2-Ph	**24**	^{t}Bu	NMe_2-Ph

Results

Synthesis of Fe(II) Compounds. The α-diimine ligands, $^{R',R''}[N,N]$, (where $^{R',R''}[N,N]$ = R′−N═CR″−CR″═N−R′, R′ = *tert*-butyl (*t*Bu), cyclohexyl (Cy), and R″ = phenyl (Ph), *para*-fluorophenyl (F−Ph), *para*-bromophenyl (Br−Ph), *para*-methylphenyl (Me−Ph), *para*-methoxyphenyl (MeO−Ph), *para*-dimethylaminophenyl (NMe_2−Ph)) were prepared via the modification of a literature procedure,[55] using $TiCl_4$ as an activating agent (Scheme 2). After aqueous workup, the crude residues were recrystallized from hot alcohol to give the desired products in good isolated yields (65−85%).

For the Fe(II) chloride complexes, **13**−**24**, the addition of CH_2Cl_2 to an intimate mixture of the pro-ligand and $FeCl_2(THF)_{1.5}$ produced deep blue solutions, except in the case of **18** and **24**, which were red-brown (Scheme 3). After stirring overnight, the solutions were filtered and concentrated before the desired product was obtained as a purple or red-brown solid, following precipitation with pentane. Magnetic moment measurements (Evans' NMR method) on **13**−**24** revealed high-spin Fe(II) centers with μ_{eff} in the range 4.93−5.28 μ_B. Despite the paramagnetism of the complexes, contact-shifted ^{1}H NMR spectra could be obtained for each compound and assigned on the basis of integrated signal intensities and chemical shifts. The imine $\nu_{C=N}$ stretch was visible between 1600 and 1611 cm^{-1}, and FAB-MS showed the expected $[M+H]^+$ peaks as well as common fragments, such as $[M-Cl]^+$. In addition, crystals suitable for X-ray structure analysis of **13**, **14**, **18**−**20**, and **24** were obtained. The complexes were found to possess closely related monomeric solid-state structures with four-coordinate metal centers.

As an example, crystals suitable for X-ray analysis were obtained through slow cooling of a saturated solution of **13** in toluene. The X-ray crystal structure of **13** revealed a C_S-symmetric complex with a highly distorted tetrahedral iron center, where the cis angles are in the range of 78.43(15)−125.62(7)°, with the most acute being the bite angle of the chelating *N*,*N*′ ligand (Figure 1). The crystallographic mirror plane includes the iron center and the two chlorines and bisects the C(1)−C(1A) single bond [1.521(6) Å] between

(55) Kimpe, N. D.; D'Hondt, L.; Stanoeva, E. *Tetrahedron Lett.* **1991**, *32*, 3879.

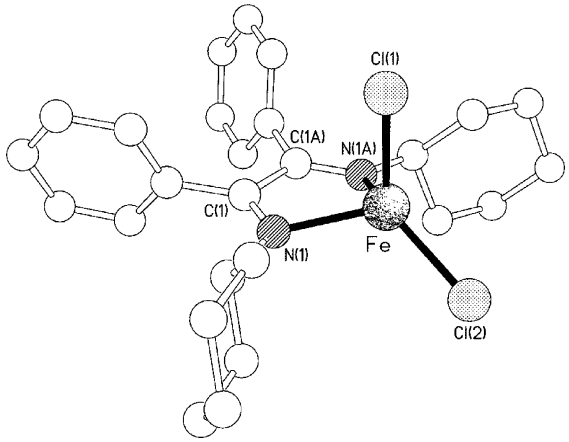

Figure 1. The molecular structure of the C_S-symmetric **13**. Selected bond lengths (Å): Fe−Cl(1), 2.2551(16); Fe−Cl(2), 2.2183(15); Fe−N(1), 2.077(3); Fe−N(1A), 2.077(3); N(1)−C(1), 1.284(4); C(1)−C(1A), 1.521(6). Selected bond angles (°): Cl(1)−Fe−Cl(2), 125.62(7); Cl(1)−Fe−N(1), 101.79(9); Cl(1)−Fe−N(1A), 101.79(9); Cl(2)−Fe−N(1), 119.24(9); Cl(2)−Fe−N(1A), 119.24(9); N(1)−Fe−N(1A), 119.24(9).

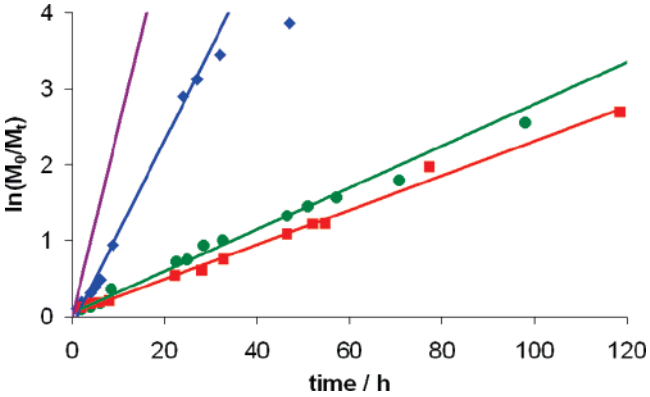

Figure 2. Plot of $\ln(M_0/M_t)$ versus time for the bulk polymerization of styrene (200 equiv, 1-PECl, 120 °C) by $^{Cy,R''}[N,N]FeCl_2$ complexes (R″ = *p*-F−Ph, ■; R″= Ph, ●; R″ = *p*-Br−Ph, ♦). $^{Cy,H}[N,N]FeCl_2$ rate (purple line) included for reference purposes.[7]

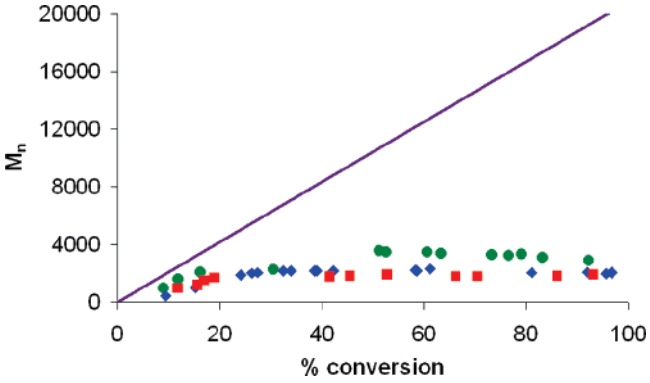

Figure 3. Plot of molecular weight versus conversion for the bulk polymerization of styrene (200 equiv, 1-PECl, 120 °C) by $^{Cy,R''}[N,N]FeCl_2$ complexes (R″ = *p*-F−Ph, ■; R″ = Ph, ●; R″ = *p*-Br−Ph, ♦).

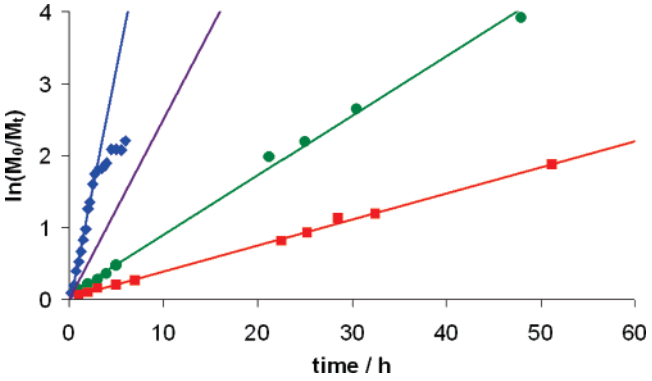

Figure 4. Plot of $\ln(M_0/M_t)$ versus time for the bulk polymerization of styrene (200 equiv, 1-PECl, 120 °C) by $^{Cy,R''}[N,N]FeCl_2$ complexes (R″ = *p*-Me−Ph, ■; R″ = *p*-MeO−Ph, ●; R″ = *p*-NMe_2−Ph, ♦). $^{Cy,H}[N,N]FeCl_2$ rate (purple line) included for reference.[7]

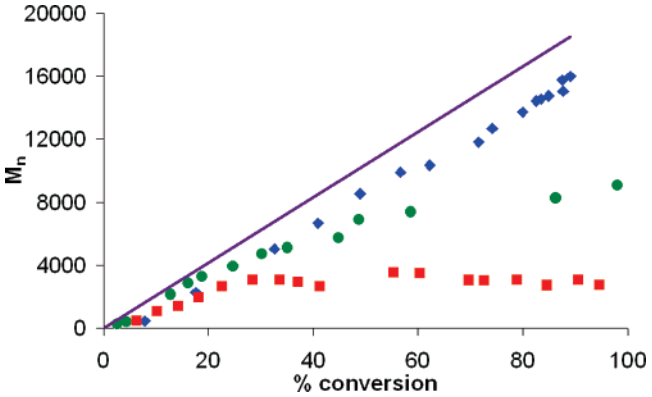

Figure 5. Plot of molecular weight versus conversion for the bulk polymerization of styrene (200 eq., 1-PECl, 120 °C) by $^{Cy,R''}[N,N]FeCl_2$ complexes (R″ = *p*-Me−Ph, ■; R″ = *p*-MeO−Ph, ●; R″ = *p*-NMe_2−Ph, ♦).

Scheme 4

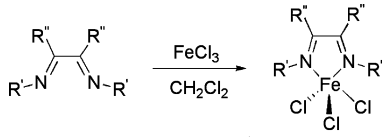

	R′	R″
25	Cy	Ph
26	Cy	F-Ph
27	Cy	Br-Ph
28	Cy	Me-Ph
29	Cy	MeO-Ph
30	Cy	NMe_2-Ph

	R′	R″
31	^{t}Bu	H
32	^{t}Bu	Ph
33	^{t}Bu	F-Ph
34	^{t}Bu	Br-Ph
35	^{t}Bu	Me-Ph
36	^{t}Bu	MeO-Ph
37	^{t}Bu	NMe_2-Ph

the two imine units [C(1)−N(1) 1.284(4) Å]. The two imines are perfectly coplanar (a consequence of the mirror symmetry), and the iron perches above this plane by ca. 0.59 Å in the direction of Cl(1). The $FeCl_2$ unit adopts a conformation that puts Cl(1) in a pseudo-apical position and Cl(2) in a pseudo-basal position, such that Cl(1) is ca. 2.83 Å above the diimine plane, whereas Cl(2) is only ca. 0.50 Å below it. Associated with this is an elongation of the Fe−Cl(1) bond length [2.2551(16)] cf. that to Cl(2) [2.2183(15) Å]; the angle between the two chlorine atoms is substantially enlarged from ideal tetrahedral, being 125.62(7)°. The aryl rings on the backbone are slightly twisted away from orthogonal; the torsion angle about the C(1)−C(Ph) bond is ca. 102°, and

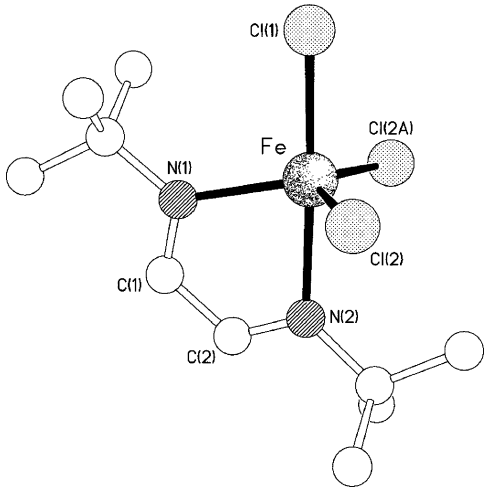

Figure 6. Molecular structure of one (**I**) of the two crystallographically independent C_S-symmetric complexes present in the crystals of **31**.

the top [Cl(1) side] of the phenyl rings is rotated away from the mirror plane. The closely related structures, **14**, **18**−**20**, and **24** can be found in the Supporting Information.

Polymerization Studies. 13−**24** were tested for the ATRP of styrene (200 equiv, bulk), under an inert atmosphere at 120 °C, using 1-phenylethyl chloride (1-PECl) as the initiator. As seen previously with the fluorophenyl derivatives,[6] complexes bearing electron withdrawing groups in the para position of the phenyl ring (**13**, **14**, **19**, and **20**) resulted in polymerizations that proceeded slowly. Figure 2 shows the rate data for **13**−**15**, along with $^{Cy,H}[N,N]FeCl_2$ for comparison. They required ca. 70 h to reach 80% conversion, with pseudo-first-order rate constants of 0.01−0.03 h^{-1}. This is significantly slower than the aldimine derivatives, which reached high conversions within 24 h, with rate constants in the range of 0.25−0.27 h^{-1}.[7]

The molecular weight data on polystyrene samples generated using these catalysts revealed that the predominant mechanism of polymerization was not ATRP. Low-molecular-weight polymers were isolated, with molecular weights independent of conversion (Figure 3) and consistent with the operation of a CCT mechanism. End-group analyses by ^{1}H NMR spectroscopy revealed the presence of olefinic end-groups at 6.1−6.4 ppm, with no evidence for the chlorine-terminated chains expected from an ATRP mechanism (~4.6).

Substituting the para position of the phenyl ring with a more electron-donating group gave complexes that showed a trend back toward typical ATRP behavior. In the case of *p*-Me−Ph substituted complexes, **16** and **22**, rates are still relatively slow (0.04−0.06 h^{-1}), and the molecular weight data do not increase linearly with conversion. End-group analyses confirmed the presence of vinylene end-groups, consistent with CCT. Replacing the methyl group by a methoxy substituent increased the rate to 0.10 for **17** and 0.07 h^{-1} for **23**, and molecular weights showed an initial linear increase with conversion. A limit is reached, at around 8000 Da, and the polymer showed only olefin end-groups, with no signals in the ^{1}H NMR spectrum that were characteristic of a halogen end-group. The most electron-

Table 1. Selected Bond Lengths (Angstroms) and Angles (Degrees) for the Two Crystallographically Independent C_S-Symmetric Complexes (**I** and **II**) Present in the Crystals of **31**

	Mol I	Mol II		Mol I	Mol II
Fe−Cl(1)	2.285(3)	2.294(3)	Fe−Cl(2)	2.2053(19)	2.2109(19)
Fe−N(1)	2.145(6)	2.141(6)	Fe−N(2)	2.243(7)	2.275(7)
Fe−Cl(2A)	2.2053(19)	2.2109(19)	N(1)−C(1)	1.272(10)	1.276(9)
C(1)−C(2)	1.455(12)	1.456(12)	N(2)−C(2)	1.247(9)	1.265(9)
Cl(1)−Fe−Cl(2)	94.13(6)	94.68(7)	Cl(1)−Fe−N(1)	100.65(19)	98.7(2)
Cl(1)−Fe−N(2)	177.83(19)	176.4(2)	Cl(1)−Fe−Cl(2A)	94.13(6)	94.68(7)
Cl(2)−Fe−N(1)	114.76(7)	117.06(7)	Cl(2)−Fe−N(2)	86.82(10)	87.03(11)
Cl(2)−Fe−Cl(2A)	127.08(14)	122.69(13)	N(1)−Fe−N(2)	77.2(2)	77.7(2)
N(1)−Fe−Cl(2A)	114.76(7)	117.06(7)	N(2)−Fe−Cl(2A)	86.82(10)	87.03(11)

donating substituent, *p*-NMe_2−Ph, results in catalysts with extremely fast polymerization rates (0.72 for **18** and 0.36 h^{-1} for **24**), and the molecular weight now increases linearly with conversion. End-group analyses on precipitated polystyrene samples revealed that the polymer is halogen terminated, with no olefin peaks detectable. Rate data and plots of M_n versus conversion for **16**−**18** are shown in Figures 4 and 5, respectively.

The rate of polymerization for **18**, at 0.72 h^{-1}, is the highest found to date in the α-diimine system, reaching 85% conversion within 3 h, some three times faster than the aldimine α-diimine catalyst, ^{Cy,H}[*N*,*N*]$FeCl_2$, (0.25 h^{-1}). Molecular weights for **18** do not match-up perfectly with theoretical values, being consistently ca. 10−20% lower than expected. This is attributed to a small amount of termination through CCT, giving olefin-terminated oligomers, which are not reincorporated into the polymer. The PDIs range from 1.2 to 1.3 until around 75% conversion, where they broaden to 1.4, and it is notable that the GPC traces show an asymmetry, tailing toward low molecular weight and supporting the occurrence of a small amount of chain transfer (Figure S44 in the Supporting Information). GC-MS and ^{1}H NMR spectroscopy on the hydrocarbon-soluble fraction of the crude polymer confirmed the presence of small amounts of olefin-terminated products.

Similar trends to those described above are seen in the rates and molecular weight data for the *t*Bu derivatives, **19**−**24**. Incorporation of electron-withdrawing groups into the ligand backbone results in a low-molecular-weight, olefin-terminated polymer, whereas electron-donating groups tend back toward ATRP behavior. These data are included in the Supporting Information.

Synthesis of Fe(III) Compounds. In our preliminary report,[6] we showed that a key factor in determining the differing radical polymerization mechanisms catalyzed by α-diimine iron catalysts is the spin-state of the metal in the oxidized Fe(III) species present in the ATRP equilibrium, high-spin centers, giving rise to ATRP, whereas intermediate-spin centers afforded CCT behavior. To further explore the origin of the differing polymerization mechanisms observed using aryl-substituted Fe(α-diimine) catalysts, Fe(III) derivatives were targeted and prepared according to Scheme 4. Careful control over the reaction conditions was required to ensure the desired products were obtained in high purity.

Unlike their Fe(II) counterparts, **25**−**37** did not give meaningful ^{1}H NMR spectra. Evans' NMR measurements revealed μ_{eff} values for **25**−**29** and **32**−**36** in the range of 3.9−4.2 μ_B, close to the intermediate ($S = {}^3/_2$) spin value of 3.87,[56] whereas **30**, **31**, and **37** have values in the range of 5.6−5.8 μ_B, consistent with high-spin Fe(III) centers. More detailed studies on **25**−**31** are in progress using SQUID, EPR, and Mössbauer spectroscopy and will be reported in due course.

X-ray structures of L_nFeCl_3 species are surprisingly rare, and there are only a few examples of crystallographically characterized five-coordinate iron trichloride complexes incorporating nitrogen donors.[57,58] Crystals of **31** suitable for X-ray analysis were obtained through slow evaporation of a solution of ^{tBu,H}[*N*,*N*]$FeCl_3$ in $CDCl_3$/cyclohexane (95:5 v/v) and comprised two crystallographically independent C_s symmetric molecules; molecule **I** is shown in Figure 6 and molecule **II** in Figure S26 in the Supporting Information. The two molecules have essentially identical geometries (Table 1), the rms fit of the non-hydrogen atoms being ca. 0.05 Å. The mirror plane contains the iron center, the two imine units, and Cl(1). The geometry at the iron is distorted trigonal bipyramidal, with Cl(1) and N(2) in the axial positions; the metal lies ca. 0.23 [0.23 Å] out of the equatorial {N(1),Cl(2),Cl(2A)} plane (the value in square parentheses refers to molecule **II**). The bite of the *N*,*N*′ chelating ligand is slightly contracted compared to that seen in **13**, 77.2(2)° [77.7(2)°] in the case of **31**, cf. 78.43(15)° in **13**. For both the chlorines and the nitrogens, it is noticeable that the axial bonds, (Fe−Cl(1) 2.285(3) [2.294(3) Å], Fe−N(2) 2.243(7) [2.275(7) Å]) are longer than their equatorial counterparts (Fe−Cl(2) 2.2053(19) [2.2109(19) Å], Fe−N(1) 2.145(6) [2.141(6) Å]). The C−C bond between the imine units is noticeably shorter here (1.455(12) [1.456(12) Å]) than in **13** (1.521(6) Å), possibly due to a lesser steric repulsion between the carbon substituents (protons in **31** compared to phenyls in **13**).

The intermediate-spin complexes **25**−**29** and **32**−**36** could not be characterized crystallographically because of their instability in both the solid and solution states. These compounds were found to be sensitive to light, air, and moisture, and control over the concentration, time, and

(56) The lower μ_{eff} values observed for these Fe(III) complexes could also be due to a mixed spin system or spin admixture, rather than a pure $S = {}^3/_2$ spin-state. However, the presence of the lower spin-state species undoubtedly correlates with the differing polymerization behavior.

(57) Daran, J.-C.; Jeannin, Y.; Martin, L. M. *Inorg. Chem.* **1980**, *19*, 2935.
(58) Millington, K. R.; Wade, S. R.; Willey, G. R. *Inorg. Chim. Acta* **1984**, *89*, 185.

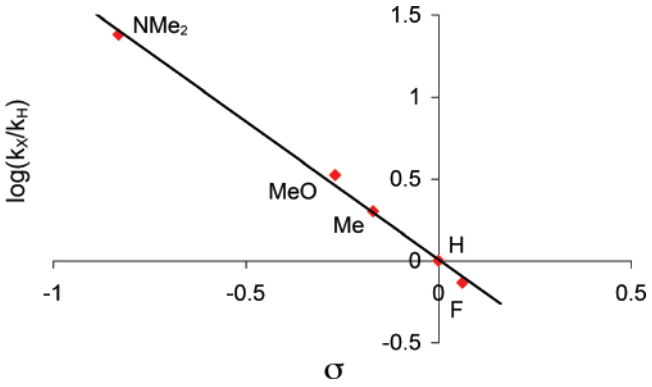

Figure 7. Hammett plot showing the correlation between the substituent constant and the rate of styrene polymerization for $^{Cy,R''}[N,N]FeCl_2$ catalysts.

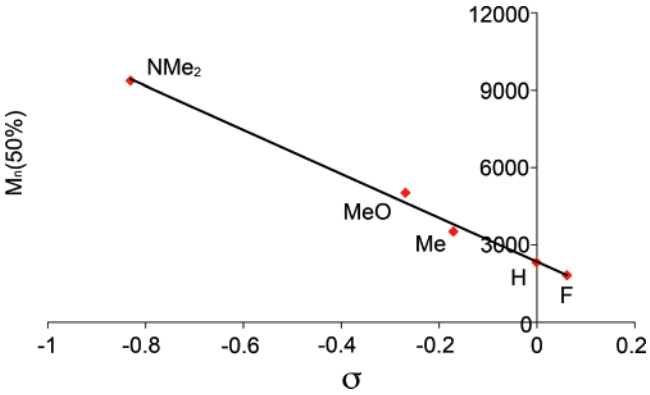

Figure 8. Hammett plot showing the correlation between the substituent constant and the molecular weight of polystyrene at 50% conversion for $^{Cy,R''}[N,N]FeCl_2$ catalysts.

temperature of a reaction was necessary to isolate pure complexes. This is not unexpected because a decrease in the halogenophilicity of the parent Fe(II) complexes would potentially promote the decomposition (via halogen loss) and disproportionation reactions of the intermediate-spin Fe(III) species. Attempts to crystallize the dark-purple complex $^{t\text{Bu,FPh}}[N,N]FeCl_3$, **33**, resulted in the formation of red crystals, whose X-ray structures showed that two molecules of $^{t\text{Bu,F-Ph}}[N,N]FeCl_3$ had disproportionated to form $^{t\text{Bu,F-Ph}}[N,N]FeCl_2$, $FeCl_4^-$ and $^{t\text{Bu,F-Ph}}[N,N]H^+$, **38** (Figure S28, Supporting Information).

Discussion

Correlation of the Metal Spin-State with the Polymerization Mechanism. Previous work showed that $^{Cy,H}[N,N]FeCl_3$ exhibited a solution magnetic moment of 5.97 μ_B, corresponding well with the spin-only value of 5.92 μ_B for a d^5-high-spin Fe(III) center ($S = {}^5/_2$, sextet). In contrast, the magnetic moment of the *N*-aryl derivative $^{DiPP,H}[N,N]FeCl_3$ (where DiPP is 2,6-di*iso*propylphenyl) was 3.99 μ_B, correlating well to a d^5-intermediate-spin Fe(III) center (3.87 μ_B, $S = {}^3/_2$, quartet).[59] The magnetic moments for the majority of the 2,3 aryl-substituted derivatives **25**−**29** and **32**−**36** were found to lie in the range 3.9−4.2 μ_B, consistent with intermediate-spin Fe(III) centers, whereas the solely alkyl-substituted complex, **31**, was high-spin ($\mu_{eff} = 5.81\ \mu_B$). Interestingly, the *para*-dimethylamino substituted complexes, **30** and **37**, also exhibited solution magnetic moments consistent with high-spin Fe(III) centers. This difference in spin-state correlates well with the evident switch in polymerization mechanism, high-spin species catalyzing ATRP, whereas the lower-spin species give rise to polymers via CCT. Evans' method determinations of μ_{eff} for **26** at elevated temperatures confirmed that the lower spin-state is maintained at the polymerization temperature of 120 °C.

The expected geometric differences between the sextet and quartet spin-states are reproduced in the solid-state structure of **31**. The Hartree−Fock calculations presented previously[6] suggest that a change in spin-state should be visible in the solid-state structures of the complexes, due to a distortion of the antiperiplanar nitrogen donor bond parameters. The calculations predict an increase in the Cl(2)−Fe−Cl(2)* angle by approximately 10° in the quartet system and also show a significant difference in the Fe−N(2) bond lengths between the congeners, with the 2.31 Å sextet state being 0.24 Å longer than the 2.07 Å quartet state. Complexes with $S = {}^5/_2$, sextet, structures are predicted to exhibit trigonal bipyramidal structures, whereas $S = {}^3/_2$, quartet, complexes should favor a more square-pyramidal geometry. The Fe−N(2) bond length obtained from the solid-state structure is 2.24 Å, correlating well with the sextet spin-state, and the geometry at the iron center is best described as trigonal bipyramidal.

The Effect of Para-Substituted Phenyl Substituents on the Observed Polymerization Mechanism. Incorporating electron-withdrawing aryl groups into the diimine backbone results in a switch of the polymerization mechanism from ATRP toward CCT, despite the presence of the ATRP-directing *N*-alkyl donor. When the more electron-withdrawing *para*-fluorophenyl substituents are incorporated, there is a greater prevalence of CCT, the rate is decreased, and the polymer obtained is of even lower molecular weight (M_n ~1800 for $^{Cy,F-Ph}[N,N]FeCl_2$, cf. M_n ~3400 for $^{Cy,Ph}[N,N]FeCl_2$, corresponding to approximately 17 versus 33 monomer insertions, respectively). Because the radical concentration is determined by the interplay of the ATRP and CCT equilibria, it is not possible, without extensive modeling, to employ Mayo plots to determine the chain-transfer constants. The effect of these equilibria on the radical concentration in the polymerization medium is discussed in a separate study, which also addresses the role of organometallic intermediates in these processes.[53]

Switching to an electron-donating group at the para position of the phenyl ring results in an increase both in rate and in the molecular weight of the polymer obtained (the peak molecular weight is ~3500 for $^{Cy,Me-Ph}[N,N]FeCl_2$, cf. M_n ~7000 for $^{Cy,MeO-Ph}[N,N]FeCl_2$, corresponding to approximately 34 vs 67 monomer insertions, respectively). When a strongly electron-donating group is installed in the para position, as in the case of $^{Cy,NMe2-Ph}[N,N]FeCl_2$, the mechanism switches back to ATRP, and the rate is further increased to the highest value recorded within this (α-diimine)Fe catalyst family. The equilibria between the two

(59) Gibson, V. C.; O'Reilly, R. K.; Rzepa, H. S.; Shaver, M. P. *Polym. Prepr. (Am. Chem. Soc., Div. Polym. Chem.)* **2005**, *46*, 160.

competing mechanisms are clearly finely balanced; small changes to the electronic characteristics of the ligand backbone dramatically affect the prevalence of ATRP versus CCT polymerization pathways.

There is a clear correlation between the nature of the para substituent of the phenyl ring in the 2,3-aryl substituted complexes and both the rate of styrene polymerization and molecular weight of polystyrene obtained. As the para substituent becomes more electron-donating, the rate of polymerization increases, and the peak molecular weight for the complexes terminating through CCT is higher. Hammett plots of substituent constant versus $\log(k_X/k_H)$ (Figure 7) and of the polymer molecular weight at 50% conversion (Figure 8) show good linearity for $^{Cy,R''}[N,N]FeCl_2$ catalysts.

Conclusions

A series of new α-diimine ligands has been synthesized through the $TiCl_4$-activated condensation of the requisite ketone and amine. Fe(II) and Fe(III) complexes of these ligands have been prepared and characterized, including the first α-diimine $FeCl_3$ complex to be crystallographically characterized. The catalytic reactivity of the Fe(II) dichloride complexes has been investigated through styrene polymerization studies, and the prevalent polymerization mechanism has been shown to correlate with the spin-state of the Fe(III) trichloride species. Incorporating an electron-withdrawing group, such as Ph or F−Ph, at the 2,3 positions of the ligand backbone switches the polymerization mechanism from ATRP to CCT, even in the presence of ATRP-directing alkylimino donors. Substituting the para position of the aryl group on the 2,3 position of the ligand backbone with electron-donating substituents switches the polymerization mechanism back to ATRP. The Hammett substituent constant, σ, correlates well with both the rate of styrene polymerization and the peak molecular weight of the isolated polymer, illustrating a structure−reactivity relationship that could prove useful in the future design of selective catalysts based on metal spin-state.

Experimental Section

General Experimental Procedures. All of the manipulations of air and/or moisture-sensitive compounds were carried out under nitrogen using standard Schlenk and cannula techniques or in a conventional nitrogen-filled glovebox. Elemental analyses were performed by the microanalytical service of the chemistry department of London Metropolitan University. Crystal data were collected on Oxford Diffraction Xcalibur 3 and PX Ultra diffractometers. NMR spectra were recorded on Bruker AC250 (^{1}H, 250.1 MHz; ^{13}C, 60.9 MHz), DRX400 (^{1}H, 400.1 MHz; ^{13}C, 100.6 MHz), and AV-400 (^{1}H, 400.3 MHz; ^{13}C, 100.7 MHz) spectrometers, at 293 K unless otherwise stated. ^{1}H and ^{13}C chemical shifts are reported as δ and referenced to the residual proton signal and to the ^{13}C signal of the deuterated solvent, respectively. The following abbreviations have been used for multiplicities: s (singlet), d (doublet), t (triplet), m (unresolved multiplet); coupling constants are reported in hertz. Infrared spectra were obtained as nujol mulls on chemical ionization (CI) plates or as KBr discs on a PerkinElmer 1710X FTIR spectrometer. FAB, electron ionization, and CI mass spectra were recorded on Micromass AutoSpec Premier and VG Platform spectrometers at Imperial College London. GPC data were collected using *Cirrus GPC/SEC* software, ver. 1.11, connected to a Shodex RI-101 detector and were referenced to polystyrene standards (PolymerLabs EasiCal, PS1). Solvents were dried by refluxing over an appropriate drying agent and distilling or passing through a cylinder filled with commercially available Q-5 catalyst (13% Cu(I) oxide on Al_2O_3) and activated Al_2O_3 (3 mm, pellets) in a stream of nitrogen and were degassed before use. NMR solvents were dried over molecular sieves and degassed prior to use. Styrene was stirred over calcium hydride for 24 h, vacuum-transferred, degassed, and then stored in an inert atmosphere at −35 °C. Diazadiene ligands RN═CH−CH═NR, where R = *t*Bu or Cy, were prepared in bulk through modification of the literature procedures[7,8,60] and purified through recrystallization. $FeCl_2(THF)_{1.5}$ was synthesized according to literature procedures.[61] $FeCl_3$ was purchased from Aldrich Chemical Co. and used as received. All of the amines were freshly distilled before use.

Table 2. Crystal Data, Data Collection, and Refinement Parameters for **13** and **31**[a]

data	13	31
formula	$C_{26}H_{32}Cl_2FeN_2$	$C_{10}H_{20}Cl_3FeN_2$
solvent	0.5MeOH	
fw	515.31	330.48
color, habit	purple needles	orange needles
cryst size (mm)	0.36 × 0.12 × 0.04	0.35 × 0.01 × 0.01
T (K)	173	173
cryst syst	tetragonal	orthorhombic
space group	$P\bar{4}2_1m$ (no. 113)	$Cmc2_1$ (no. 36)
a (Å)	20.3559(6)	10.2994(13)
b (Å)		19.845(3)
c (Å)	6.5223(4)	14.723(2)
α (deg)		
β (deg)		
γ (deg)		
V (Å^3)	2702.6(2)	3009.2(7)
Z	4[b]	8[c]
D_c (g cm^{-3})	1.266	1.459
radiation used	Mo Kα	Mo Kα
μ (mm^{-1})	0.774	1.513
2θ max (deg)	65	66
no. of unique reflns measured	4873	4282
obs, $\|F_o\| > 4\sigma(\|F_o\|)$	4722	2870
no. of variables	164	175
R_1, wR_2[d]	0.077, 0.173	0.097, 0.099

[a] Details in common: graphite monochromated radiation, refinement based on F^2. [b] The complex has crystallographic C_S symmetry. [c] There are two crystallographically independent C_S-symmetric complexes in the asymmetric unit. [d] $R_1 = \sum||F_o| - |F_c||/\sum|F_o|$; $wR_2 = \{\sum[w(F_o^2 - F_c^2)^2]/\sum[w(F_o^2)^2]\}^{1/2}$; $w^{-1} = \sigma^2(F_o^2) + (aP)^2 + bP$.

Polymerization Procedures. All of the polymerizations were set up and performed under an atmosphere of oxygen-free, dry nitrogen. A solution of monomer, initiator, and catalyst (200:1:1; $[M]_0 = 8.73$ M, $[I]_0 = 0.044$ M, $[cat] = 0.044$ M) was added to a 30 mL ampule equipped with a magnetic stirrer bar. The ampules were heated in a sand bath, at 120 °C, with magnetic stirring. After stirring for the allotted period of time (15 min−2 h), an aliquot (0.1 mL) was removed. Conversion was determined by integration of the monomer versus polymer backbone resonances in the ^{1}H NMR spectrum of the crude product in $CDCl_3$. Once the reaction was completed, the contents of the ampules were dissolved in THF and added dropwise to an approximately 20-fold excess of rapidly stirred acidified methanol (1% HCl v/v). The precipitate that formed

(60) Hsieh, A. T. T.; West, B. O. *J. Organomet. Chem.* **1976**, *112*, 285.
(61) Cotton, F. A.; Luck, R. L.; Son, K.-A. *Inorg. Chim. Acta* **1991**, *179*, 11.

was filtered off and washed with methanol. The precipitate was dried for 24 h under a vacuum. Samples were analyzed by GPC.

X-ray Crystallographic Analyses. Table 2 provides a summary of the crystallographic data for **13** and **31**. Data were collected using an Oxford Diffraction Xcalibur 3 diffractometer, and the structures were refined based on F^2 using the *SHELXTL* and *SHELX-97* program systems.[62] The absolute structures of **13** and **31** were unambiguously determined by a combination of *R*-factor tests [for **13**: $R_1^+ = 0.0773$, $R_1- = 0.0860$; for **31**: $R_1^+ = 0.0969$, $R_1- = 0.1032$] and by use of the Flack parameter [for **13**: $x^+ = +0.06(3)$, $x- = +0.94(3)$; for **31**: $x^+ = +0.05(4)$, $x- = +0.95(4)$]. CCDC 627620 (**13**) and 627626 (**31**).

(62) *SHELXTL* PC version 5.1, B. A., Madison, WI, 1997; Sheldrick, G. *SHELX-97*, Institut Anorg. Chemie, Tammannstr. 4, D37077: Göttingen, Germany, 1998.

Acknowledgment. The Engineering and Physical Sciences Research Council, UK, and the Natural Sciences and Engineering Research Council, Canada, are thanked for financial support.

Supporting Information Available: Experimental details for **1**−**37**, crystallographic data for all of the reported structures (CCDC Nos. 627620−627629) and polymerization data for **19**−**24**. This material is available free of charge via the Internet at http://pubs.acs.org.

IC701500Y